Diversity focused semisyntheses of tetronate polyether ionophores

Shaoquan Lin[1,‡], Han Liu[1,‡], Esben B. Svenningsen[1], Christine N. Pedersen[1], Peter Nørby[1], Thomas Tørring[2], Thomas B. Poulsen[1,*]

[1] Department of Chemistry, Aarhus University, Langelandsgade 140, DK-8000, Aarhus C, Denmark.
[2] Department of Engineering – Microbial Biosynthesis, Aarhus University, Gustav Wieds Vej 10, DK-8000, Aarhus C, Denmark

*e-mail: thpou@chem.au.dk
‡ These authors contributed equally

Abstract

The polyether ionophores are complex natural products capable of transporting cations across biological membranes. Many family members possess highly potent antimicrobial activity and a few selected compounds have ability to target particularly aggressive cancer cells. Despite these interesting perspectives, a detailed understanding of the cellular mode-of-action of polyether ionophores is generally lacking. In principle, broad mapping of structure-activity relationships across several biological activities could provide mechanistic insights as well as identification of lead structures but access to structural diversity within the overall class is synthetically very challenging. In this manuscript, we demonstrate that novel polyether ionophores can be constructed by recycling components of highly abundant polyethers. We provide the first examples of synthetically incorporating halogen-functionalized tetronic acids as cation-binding groups into polyether ionophores and we identify analogs with strong anti-bacterial activity and minimal effects on mammalian cells.

Introduction

The polyether ionophore natural products have been a constant fix-point for organic chemistry since the 1960s.[1] The daunting complexity of compounds such as monensin, salinomycin, and X-206 challenged the abilities of chemists to identify their precise molecular structures[2,3] and has served as inspiration for the development of novel synthetic methods[4,5,6,7,8] and retrosynthetic analysis.[9] Elegant syntheses of members of this superfamily (>100 molecules) of natural products have been reported, the majority during the 1980–1990s.[10,11,12] Since then, the raison d'être of natural product synthesis has changed substantially: Ideality in synthesis-design has become a fulcrum for methodological innovation[13,14] which has also inspired remarkably efficient routes to members of the polyether ionophores.[12,15,16,17]

53 Through strategic integration[18] of complex molecule synthesis with studies of biological
54 mechanisms, the field of synthesis can catalyze new discoveries within the life sciences.
55 Diversity oriented synthesis,[19] biology oriented synthesis,[20] analogue oriented synthesis,[21]
56 diverted total synthesis,[22] complexity-to-diversity-strategies,[23] and pharmacophore-directed
57 retrosynthesis[24] are all different strategic flavors directed towards generating innovative
58 complex structures with potential pharmacological utility.[25,26]
59 The polyether ionophores have thus far escaped attention from efforts that seek to harness
60 their complex structures as fundamental entities of diversity.[2,27] There may be several reasons
61 for this, but the most important is likely that these compounds are typically considered
62 biologically uninteresting as the perturbation of ion gradients is thought to result in pleiotropic
63 effects on cellular systems. At least in eukaryotic cells, this highly simplistic view of the activity
64 of polyether ionophores is almost certainly deceptive: we do not really know in which of the
65 many endomembranes ionophores operate and which ions they transport. In fact, recent
66 discoveries concerning the biological activity of salinomycin (Sal),[28] a canonical potassium-
67 ionophore and surprising selective inhibitor of stem-like cancer cells,[29] suggest that the
68 compound does not even act as an ionophore, but instead sequesters iron in lysosomes which
69 can trigger a type of regulated oxidative cell death known as ferroptosis/oxytosis[30] or directly
70 bind protein targets as was recently shown with nucleolin.[31]
71 The main feature of polyether ionophores is their antibiotic activity and they are extensively
72 applied in the agricultural industry to control parasitic infections in poultry and as growth
73 promoters in ruminating animals.[32,33] The latter effect presumably is due to remodeling of the
74 rumen microbiota by the ionophores. Importantly, studies show that polyether ionophores do
75 not display cross-resistance with other major antibiotics and are therefore active in drug-
76 resistant bacterial strains[34] although their activity is currently restricted to gram-positive
77 strains. The lack of gram-negative activity is not mechanistically understood. As antibiotic

resistance continues to spread, agents such as the colistins, that were previously shelved due to safety issues, have now been reintroduced to the clinic. We suggest that it is due diligence to seriously consider the antibiotic potential that may lie in the polyether ionophores[34] and that the field of synthesis should consider how we can deliver truly novel molecules within this class.

Here, we outline an approach that can be used to prepare numerous novel polyether ionophores and which takes advantage of two key aspects of this class of compounds: 1) the availability of selected members – the feedstock polyether ionophores e.g. lasalocid, salinomycin, monensin – on a massive scale and 2) the overall structure of polyethers being essentially a series of connected "modules" (Figure 1a). We suggest that by disassembling these modules and then re-combining them with material made through total synthesis, we will be able to access – in a concise manner – an interesting new structural domain related to the natural polyether ionophores (Figure 1a). Some of the resulting compounds will maintain ionophore-activity, but in others, due to subtle structural alterations, this activity will be erased. As the molecular complexity will remain high such "ionophore-dead polyethers" may carry novel biological activities which – with the advent of new methods for small molecule bioactivity-profiling – it is becoming increasingly possible to explore. Importantly, this synthetic approach harnesses the tremendous knowledge generated during prior synthesis efforts for the construction of building blocks and for effecting fragment coupling.[10,11,12]

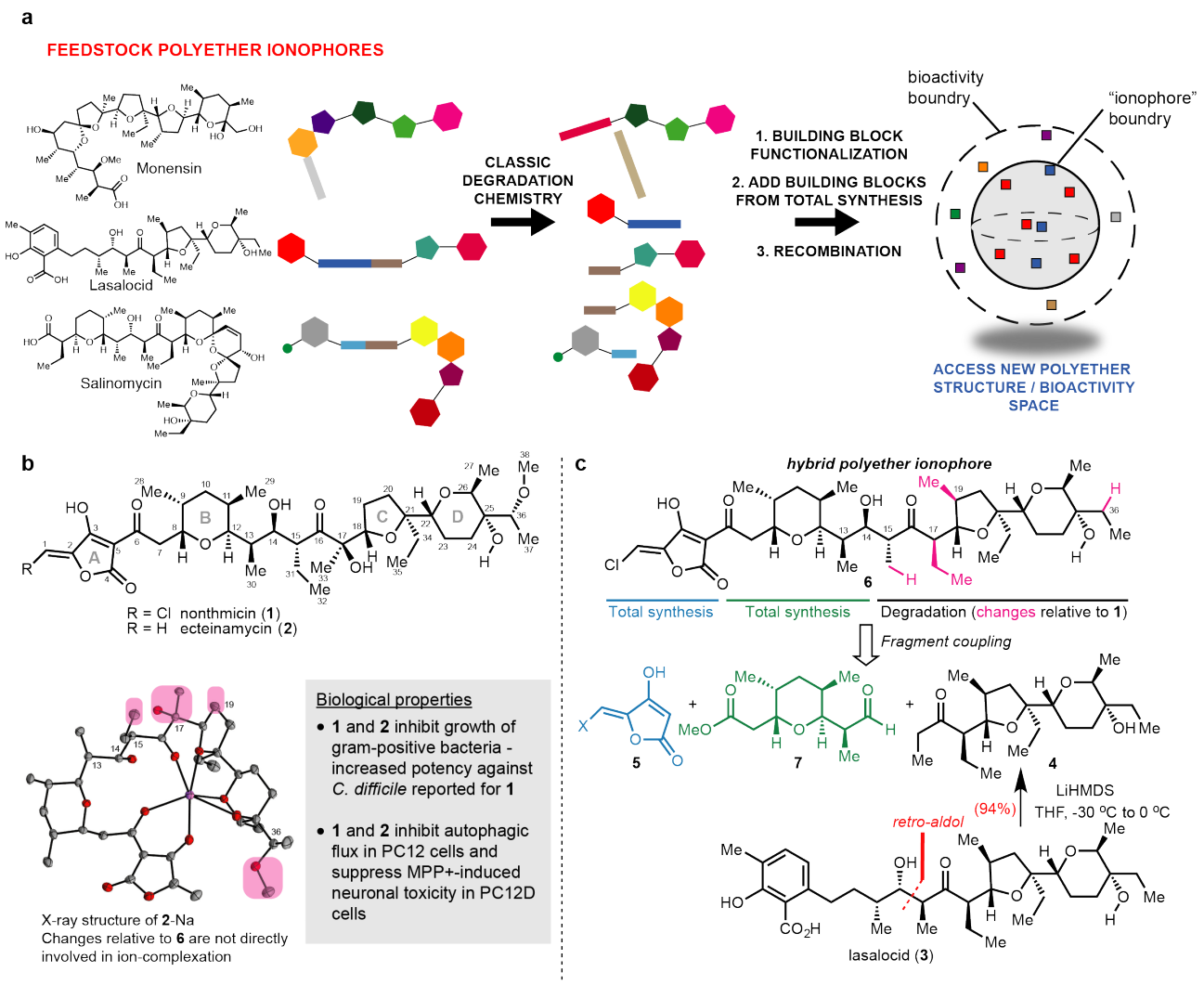

Figure 1 | Accessing structural diversity within the polyether ionophores. (a) Flowchart depicting the overall concept of reconstructing new polyether scaffolds by recycling elements from abundant feedstock polyether ionophores. The resulting "hybrid" molecules (non-red squares) are plotted in a hypothetical structure and bioactivity space to illustrate the relation of these compounds to the natural polyethers (red squares). The compounds that possess strong ionophore activity constitute a sub-space of a larger bioactivity-space that can be explored using hybrid polyethers. (b) Chemical structures and biological properties of polyether ionophores nonthmicin and ecteinamycin. The X-ray structure[35] depicts ecteinamycin bound to a single sodium-ion and chemical groups on the hydrophopic periphery that have been altered in the target hybrid polyether **6** have been circled in pink. No crystal structure of nonthmicin is available. (c) Chemical structure of the hybrid polyether **6** and

109 indication of the required fragments and the origin of these fragments. The main fragment,
110 ketone **4**, can be obtained in a single synthetic step from lasalocid.
111
112 **Results**
113 **Degradation of abundant polyether ionophores as the foundation of diversity synthesis**
114 **of complex polyethers**
115 To provide a proof-of-concept example, we placed our focus on a novel polyether ionophore,
116 nonthmicin (**1**) (Figure 1b), recently reported to possess several types of interesting biological
117 activities including antibiotic and neuroprotective activity.[35] Nonthmicin is of particular
118 interest also for structural reasons as this natural product features an unprecedented
119 chloromethylidene tetronic acid building block, that comprise the cation-binding group of the
120 molecule. Another compound, ecteinamycin (**2**), which differs from **1** only by the absence of the
121 chlorine-atom was reported almost simultaneously by the Bugni lab to be a potent anti-
122 clostridial antibiotic (Figure 1b).[36] As we carefully inspected the structure of **1** and **2**, we
123 noticed that the eastern portion (the C-D rings) displayed significant similarity to lasalocid (**3**)
124 which is available on multi-kg scale. Based on knowledge generated during the classic
125 structure-elucidation studies and then total synthesis of **3**,[37,38] we postulated that we could first
126 liberate ketone **4** through a retro-aldol reaction and then develop a short and convergent route
127 to advanced analogs of **1** (Figure 1c). Furthermore, inspection of the published X-ray crystal
128 structure of **2**-Na[35] indicated that none of the resulting structural changes (pink in Figure 1b-
129 c) would directly perturb coordination of the metal ion, at least from the solid-state structure.
130 If successful, this approach would first of all test the fundamental question if swapping modules
131 from different polyether ionophores would even be compatible with sustained antibiotic
132 activity of the resulting hybrid molecules, with **6** as the initial target structure.

133 We started our studies by optimizing the retro-aldol reaction of **3** and found that exposure to
134 LiHMDS at low temperature could result in the formation of ketone **4** in excellent yield (94%).
135 This reaction has been carried out on >10 gram scale which underscores the high availability
136 of an advanced building block such as **4**. We next focused our attention on the preparation of
137 the two remaining building blocks, tetrahydropyran-derivative **7** and the challenging
138 halomethylidene tetronic acid moiety **5** found in both **6** and **1**.
139
140 **Construction of tetrahydropyran building block**
141 The preparation of the targeted tetrahydropyran-derivative was started from (-)-2,4-
142 dimethylglutaric acid (+)-α-methylbenzylamine salt (**9**)[39,40] (Figure 2). This salt was readily
143 processed to the diol, which underwent mono-TBS protection followed by TEMPO/PhI(OAc)$_2$
144 oxidation[41] to afford aldehyde **11**. We initially proposed that the target building block could be
145 constructed via an intramolecular oxa-Michael reaction[42] following initial cross-aldol coupling
146 and Horner-Emmons reaction. However, only a trace of the cyclization product was observed
147 and this route was eventually abandoned. Inspired by the Guindon's Narasin fragment
148 synthesis,[43] we envisioned that the Mukaiyama aldol addition of a silylketene acetal to an
149 oxocarbenium intermediate could also deliver the desired tetrahydropyran-derivative.
150 Towards this end, aldehyde **11** first underwent a $CrCl_2$-catalyzed Nozaki-Hiyama-Kishi
151 crotylation reaction[44] followed by the cleavage of the silyl ether with HOAc/THF/H_2O and
152 TEMPO/PhI(OAc)$_2$-promoted lactone formation[45]. This afforded an inseparable diastereomeric
153 mixture (1.8:1, 65% isolated yield) of lactone **12** which was reduced by DIBAL-H to deliver the
154 lactol that was trapped *in situ* with Ac_2O to afford the corresponding acetate. At this stage, the
155 major diastereomer **13** – ultimately found to be the desired configuration at C12 and C13 –
156 could be isolated in 52% yield. Using $BF_3 \cdot OEt_2$ as the Lewis acid, **13** was then exposed to ((1-
157 methoxyvinyl)oxy)trimethylsilane at low temperature which provided methyl ester **14** as a

158 single diastereomer (confirmed by X-ray) in excellent yield. Finally, ozonolysis of **14** followed

159 by reductive work-up with triphenylphosphine generated aldehyde **7** (Figure 2).

160

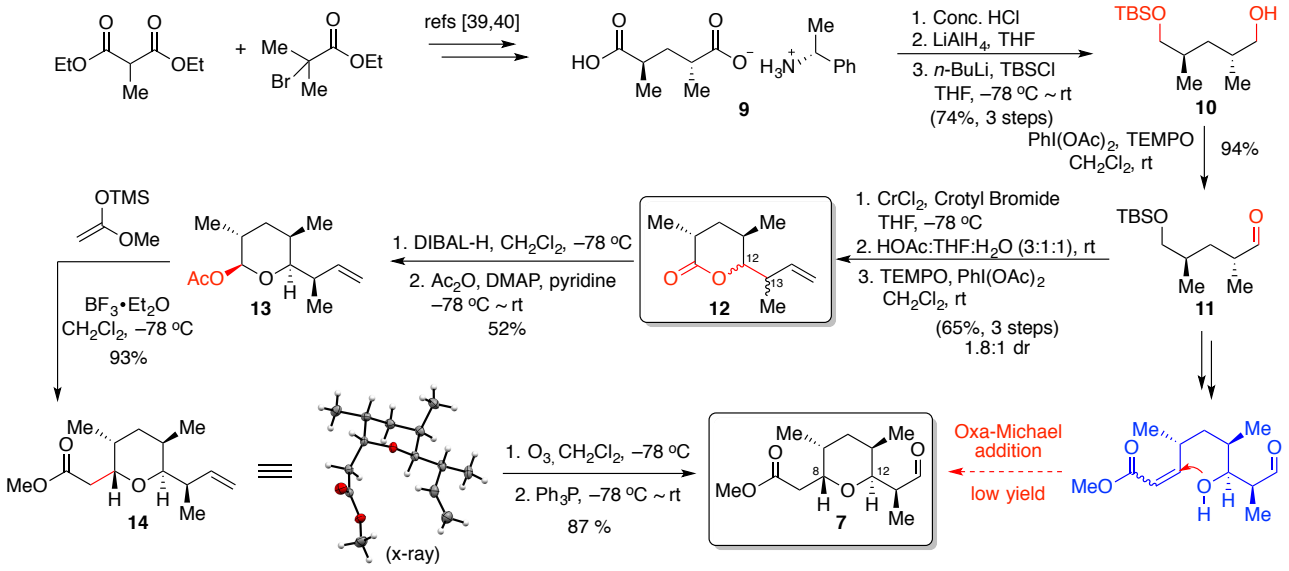

161

162 **Figure 2 |** Stereoselective synthesis of tetrahydropyran (THP) building block **7**. Two C-C

163 coupling reactions are used to construct the stereocenters at C12 and C8, the latter being a

164 highly selective addition of a silyl ketene acetal to the oxacarbenium-ion derived from **13** to

165 generate the desired *trans*-C8,C12 relative configuration. In turn, the sequence was initiated

166 from optically pure salt **9**, which is accessible via a known procedure. An alternative route to

167 closure of the THP-ring via an oxa-Michael cyclization failed. THF = tetrahydrofuran, TBSCl =

168 *tert*-butyldimethylsilyl chloride, TEMPO = (2,2,6,6-tetramethylpiperidin-1-yl)oxyl, DMAP =

169 *N,N*-dimethylpyridine-4-amine, DIBAL-H = diisobutylaluminium hydride.

170

171 **Synthesis of the halomethylidene tetronic acid building block**

172 As the most intriguing structural subunit of nonthmicin and **6**, the 3-acyl-5-chloromethylidene

173 tetronic acid became the next focus. With the overall aim to facilitate structural diversity within

174 the polyether ionophores, the ideal approach to this building block should also allow access to

175 other variants such as the methylidene and bromomethylidene species (Figure 3a). Although

176 the construction of this small and densely functionalized unit has not previously been realized,
177 published syntheses of natural products containing the nonhalogenated version provide
178 precious lessons (Figure 3b).[40-43] We opted not to pursue strategies based on organolithium
179 reagent addition[42] due to the demand of fully protected coupling partners and the uncertain
180 stability of the chlorovinyl moiety to organolithium chemistry. Likewise, approaches based on
181 the Eschenmoser methenylation[43] were not considered due to unavailability of the chlorinated
182 version of the reagent. Mindful of the presumed lability of the halomethylidene species and the
183 multiple functional groups present in the coupling partner, we selected a DCC-mediated late-
184 stage coupling as the most appealing strategy[41] and we therefore decided to target the tetronate
185 building blocks bearing an easily-removable protecting group (TMSE). After a series of
186 unsuccessful attempts (direct NMe_2/Cl exchange, construction of organotin or organoselenium
187 intermediates, see Supporting Information Figure S1 for more details), we realized the
188 synthesis of the halomethylidene tetronate via a formal C-H halogenation approach (Figure 3c).
189 The *O*-TMSE protected tetronate **19** was prepared via intramolecular Wittig cyclization[41] from
190 trityl protected α-hydroxyl TMSE ester **17** and the Bestmann reagent, and the methylidene
191 group was installed via MsCl-mediated elimination. The formal C-H halogenation was then
192 facilitated by dichlorination ($KMnO_4$-TMSCl)[44]/dibromination (Br_2)[45] of methylidene tetronate
193 and subsequent elimination (DBU) to furnish the target halomethylidene tetronates **8a** and **8b**
194 with desired (*Z*)-configuration.
195

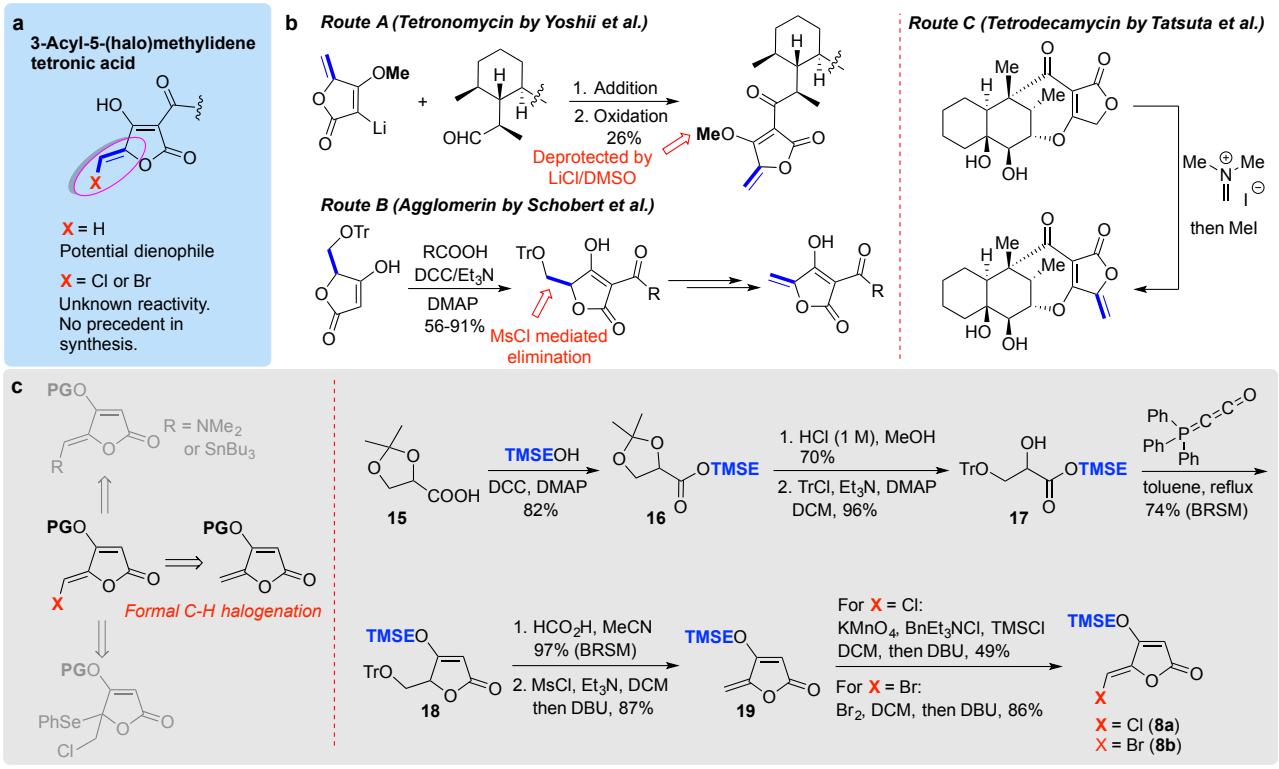

Figure 3 | Development of a synthesis of TMSE-protected 5-(halo)methylidene tetronic acid. (a) Chemical structure of the targeted 3-acyltetronic acid-derivatives found in nonthmicin/ecteinamycin and **6**. No previous syntheses of the halogenated variants have been reported. (b) Examples of known methods used to prepare non-halogenated variants. (c) From several synthesis strategies attempted (see also Figure S1, supporting information) a formal C-H halogenation of protected 5-methylidene tetronic acid was developed. Construction of the required TMSE-protected 5-methylidene precursor **19** for these reactions was carried out in 6 steps from the commercial racemic acetonide-protected glycerate **15**. This sequence allowed for preparation of both the chlorine and bromine-variants (**8a** and **8b**).

Aldol Fragment coupling

With access to the required building blocks, we initiated the fragment coupling sequence. Analysis of the composition of the stereotriad at C13-C15 in **6** suggests that the desired configuration could be achieved via the effectuation of an *anti*-aldol reaction with Felkin-control of the secondary alcohol at C14. This type of stereocontrol is usually reinforcing[46]

212 although in the present case, due to the stereogenic center at C17, double stereodifferentiation
213 in the aldol reaction is required.[47] We first attempted formation of the (*E*)-boron enolate from
214 **4** or the C25-OTES protected derivative **21** using $(c\text{Hex})_2\text{BCl-NEt}_3$ but useful conversion to the
215 enolate could not be achieved. In fact, the only known aldol reactions using **4** were carried out
216 in the classic syntheses of lasalocid **3**4 and utilized *in situ* formation of the zinc-enolate from **4**
217 which generates preferentially the configuration found in **3** – also *anti*-aldol-Felkin – and which
218 differs from the configuration needed to make **6** at all of the three stereocenters. Although this
219 aldol coupling utilized a different aldehyde compared to **7**, we evaluated the possibilities for
220 favoring the desired aldol product as being low. Consequently, we decided to instead rely on
221 the Lewis acid catalyzed Mukaiyama aldol reaction which is known to maintain Felkin-
222 selectivity. [48] Importantly, double stereodifferentiation in Mukaiyama aldol reactions is
223 established from classic studies by Evans[49] thus providing a theoretical framework for the
224 analysis of the key fragment coupling reaction. Despite the lack of very closely related reactions
225 in the literature, we expected that formation of the desired *anti*-aldol isomer (14*R*,15*R*; *anti*
226 15,17-Me↔Et) would still be challenging due to the intrinsic preference for *syn*-aldol products
227 in the Mukaiyama-aldol reaction and the combined diastereofacial bias from the stereocenters
228 already present in aldehyde **7** and ketone **4**. Formation of the *anti*-aldol products would
229 demand use of the (*Z*)-silylenolate, whereas the corresponding (*E*)-enolate could be expected
230 to reinforce the formation of a *syn*-aldol product (14*R*,15*S*; *syn* 15,17-Me↔Et). Our first
231 attempts at enolizing ketone **4** afforded some surprising results: While the (*Z*)-TES-enolate **20a**
232 could be readily formed with excess TESOTf and 2,6-lutidine with concomitant protection of
233 the tertiary alcohol at C25, formation of the corresponding (*E*)-enolate could not be accessed
234 cleanly (Figure 4a). After extensive experimentation, we found that substitution of 2,6-lutidine
235 with less hindered pyridine and inverting the sequence of reagent addition (pyridine added to
236 a pre-equilibrated solution of C25-OTES protected ketone **21** and TESOTf) could afford a nearly

237 1:1 mixture of the (*Z*)/(*E*)-TES-enolates (**20a**/**20b**) which could be partially separated by flash
238 chromatography. Gratifyingly, upon exposure of the enolates to aldehyde **7** at low temperature
239 in the presence of BF_3•OEt_2, aldol coupling proceeded in excellent yield (Figure 4b). Although
240 we could detect formation of all four putative aldol diastereomers by TLC (P1-P4 based on
241 silical gel mobility), the reaction using an enriched (ratio 1:2.3 *Z/E*) (*E*)-TES-enolate was highly
242 selective for the P3-isomer (P2: 7%, P3: 81%) whereas the pure (*Z*)-TES-enolate afforded a
243 mixture of P2 and P3 (P2: 56%, P3: 30%). Subsequent stereochemical assignment of the
244 respective compounds by X-ray crystallography revealed P3 to be the (*14R*,*15S*)-configured
245 product (**23**) in accord with the above analysis and P2 to be the desired isomer (14*R*,15*R*) (**22**).
246

247 **End game coupling and purification**

248 Both aldol products (**22** and **23**) underwent a two-step deprotection sequence, involving first
249 Olah's reagent to remove the C25-OTES group and then trimethyltin hydroxide to cleave the
250 methyl ester (Figure 4c).[50] The latter conditions were found to be critical to avoid retro-aldol
251 cleavage.

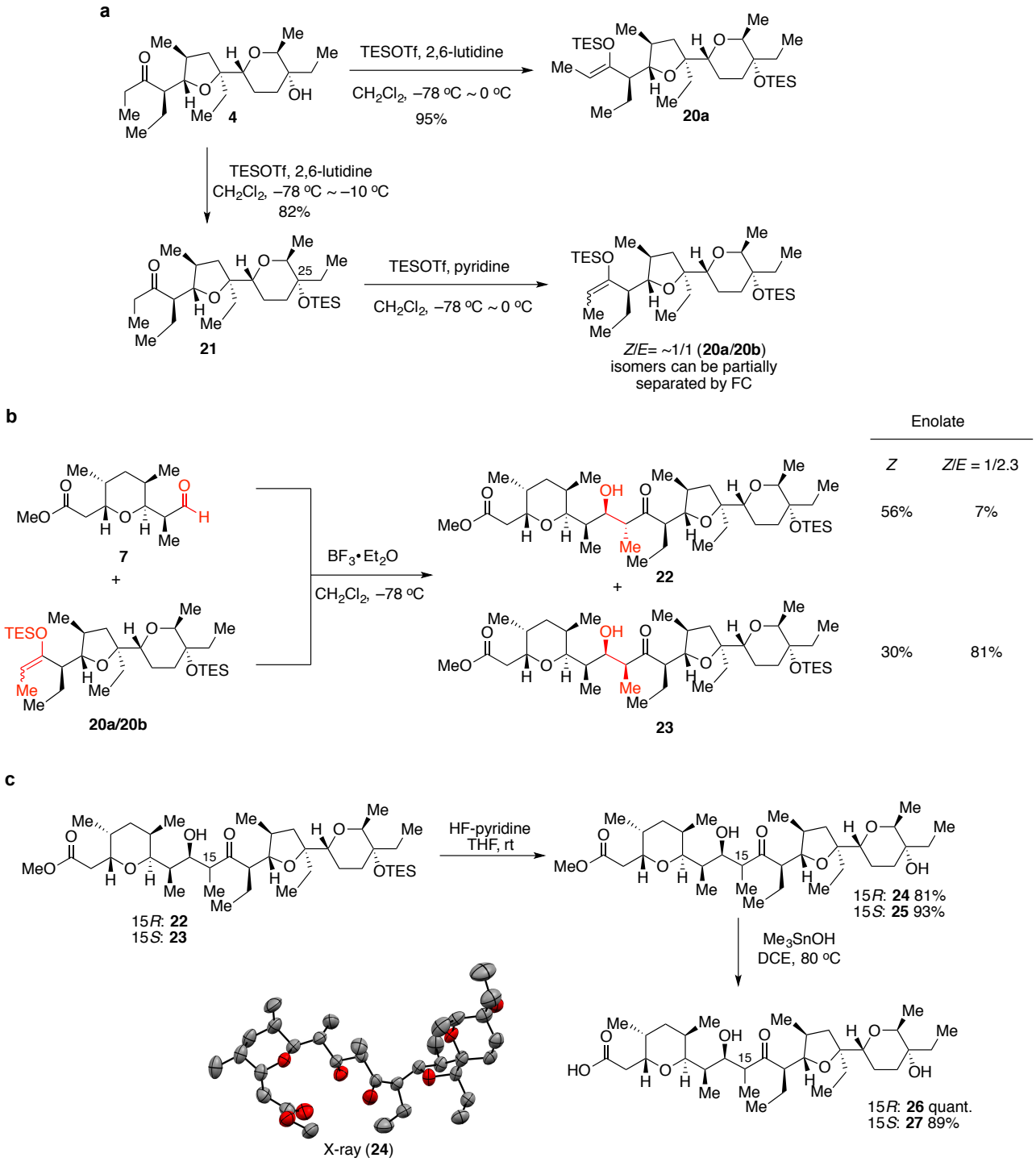

Figure 4 | Fragment-coupling via boron trifluoride-mediated Mukaiyama-aldol reaction. (a) The (*Z*)-TES-enolate **20a** could be readily obtained, but special procedures had to be developed to access mixtures of (*E*)- and (*Z*)-TES-enolates. Purification could be used to further enrich the (*E*)-TES-enolate **20b**. (b) Aldol reaction affords two major products (**22** and **23**) depending on the configuration of the silyl-enolate derived from ketone **4**. Compound **22** was confirmed by

258 X-ray analysis of derivative **24** to be the initially targeted aldol-product (c) Both aldol products
259 **22** and **23** could be processed towards the final fragment coupling in two high-yielding steps.
260 TESOTf = triethylsilyltrifluoromethanesulfonate, DCE = 1,2-dichloroethane.
261
262 With the desired acid fragments (**26** and **27**) and *O*-TMSE protected tetronates (**19** and **8a-b**)
263 in hand, we started to investigate the final fragment coupling reaction. After TBAF-mediated
264 deprotection of the *O*-TMSE group on **8a** and simple extraction, the crude tetronic acid was
265 submitted to DCC coupling with carboxylic acid **26** (Figure 5a). Fortunately, the desired product
266 **6** was smoothly formed in 24 hours with full conversion of **26**, and 59% yield (as the sodium
267 salt, **6**-Na) was obtained by preparative HPLC using MeCN-10 mM NH_4HCO_3 as eluent.[35] It is
268 worth to note that the sodium salt (formed by subsequent $NaHCO_3$ treatment and extraction)
269 show much better solubility in organic solvents than the acid form, which indicates the
270 formation of a lipophilic complex, a featured property of polyether ionophores. Encouraged by
271 this result, the bromine-analog **29** and hydrogen-analog **30**, as well as the chlorine-analog **31**
272 bearing 15-(*S*) configuration, were synthesized following the same procedure in 42-58% yields
273 (Figure 5a). We managed to prepare crystals that were suitable for X-ray diffraction from both
274 **6**, **29,** and **31** and the resulting structures revealed the formation of a cage-like structure by the
275 "naturally-configured" 15-(*R*) analogs **6** and **29** while a dimeric complex was formed by the
276 corresponding 15-(*S*)-configured compound **31**. This clearly indicates the critical role played
277 by evolutionary conformational design[51] on the cation-binding properties of the polyether
278 ionophores. Anticipating that small structural changes would potentially have a large impact
279 on the biological activities, we finally generated an additional derivative of **32** (Figure 5a) by
280 performing an *anti*-selective Evans-Saksena[52] reduction of the carbonyl group in **26** followed
281 by coupling with the tetronic acid derived from **8a** (Figure S2).

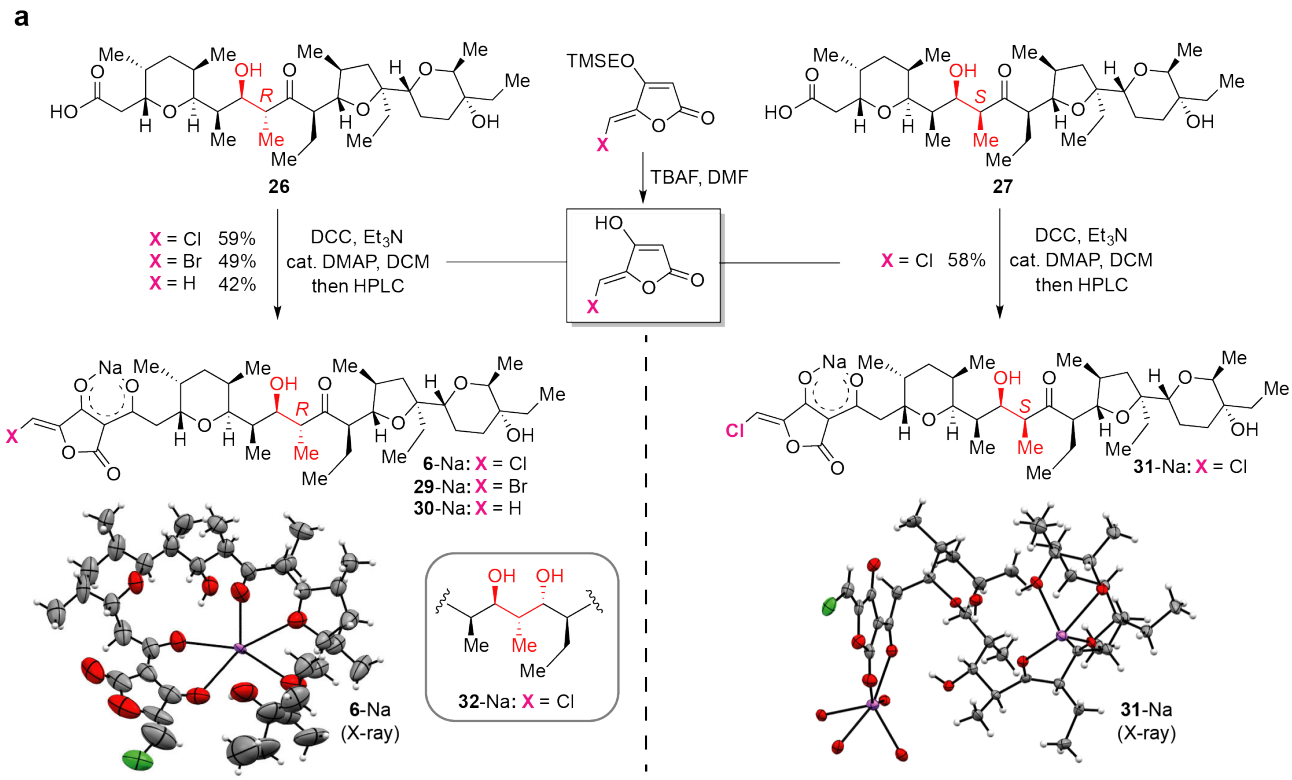

b

strain	MIC (μg/mL)							
	Lasalocid	**6**	**29**	**30**	**31**	**32**	salinomycin	vanco
S. aureus	2	8	4	32	>32	8	2	1
S. aureus MRSA USA 300 je2	2	8	8	32	>32	8-16	4	1
S. aureus ATCC 29213	4-8	8	8	32	>32	8-16	2	0.5
P. auroginosa	>32	>32	>32	nd	>32	nd	nd	>32
E. coli	>32	>32	>32	nd	>32	nd	nd	>32

cell line	IC_{50} (μM)							
	Lasalocid	**6**	**29**	**30**	**31**	**32**	salinomycin	vanco
U2OS	10±0.8	7.5±0.3	6.8±0.6	22±0.8	36±2	5.9±1.1	5.8±0.8	nd
MCF-7	6.3±2.2	16±2	13±1	26±2	42±7	6.8±0.6	4.5±1.5	nd

Figure 5. Final coupling sequence and biological activities of the hybrid tetronate polyethers. (a) Mild conditions were developed for effecting the coupling of unprotected (halo)-methylidene tetronates to acids **26** or **27**. The structures of **6**, **29** (see supporting information) and **31**, all as the sodium salts, were solved by X-ray diffraction. (b) Anti-bacterial activity and effects on mammalian cell viability were evaluated for all compounds using canonical polyether ionophores (salinomycin and lasalocid) and vancomycin as the controls. For full inhibition curves see supporting information Fig. S3 and Fig. S4. MIC-values is mean (*N=3*) and mammalian cell viability is mean ± sd (*N=3*). nd = not determined.

292 **Antibacterial and anti-proliferative activity of hybrid tetronate polyethers**

293 In order to probe the biological properties of the hybrid polyethers, we first performed an
294 evaluation of their anti-bacterial activity against a small panel of *S. aureus* strains (gram-
295 positive) and two different gram-negative strains (*P. auroginosa* and *E. Coli*). To our delight,
296 these experiments showed that compounds **6** and **29** did indeed maintain antibacterial activity
297 with a potency comparable to lasalocid and salinomycin against both wild-type and drug-
298 resistant *S. aureus* (Figure 5b and Fig. S3). Comparing the activity of **6**, **29**, and **30**, it is clear
299 that the halogen augments the contribution of the tetronic acid as the methylene-analog **30** was
300 significantly less active. Compound **31**, being epimeric to **6** at C15, was completely devoid of
301 activity (MIC >32 μg/mL), while **32** was equally active to **6**. None of the compounds were active
302 against gram-negative strains. Next, we evaluated inhibitory activity against human cancer cell
303 lines (U2OS and MCF7, Figure 5b) which afforded micromolar IC_{50}'s of all the compounds. We
304 noted however distinctively more shallow inhibition curves for the natural products, especially
305 salinomycin (Figure S4), indicating that these compounds perturb mammalian cells over a
306 larger span of concentrations.

307

308 **Bioactivity analysis using morphological profiling**

309 Modulation of cell viability is a coarse measure of the biological activity of a small molecule. To
310 provide a more nuanced analysis of the activities of the polyethers in mammalian cells, we
311 subjected all compounds to morphological profiling[53,54] in U2OS osteosarcoma cells. This
312 image-based method can generate bioactivity profiles of small molecules in an unbiased
313 manner that can be used statistically to reveal mechanistic similarities. Given the limited
314 detailed knowledge about the activity of polyether ionophores in mammalian cells, this
315 approach could potentially illuminate how structural changes impact the overall cellular
316 perturbation.

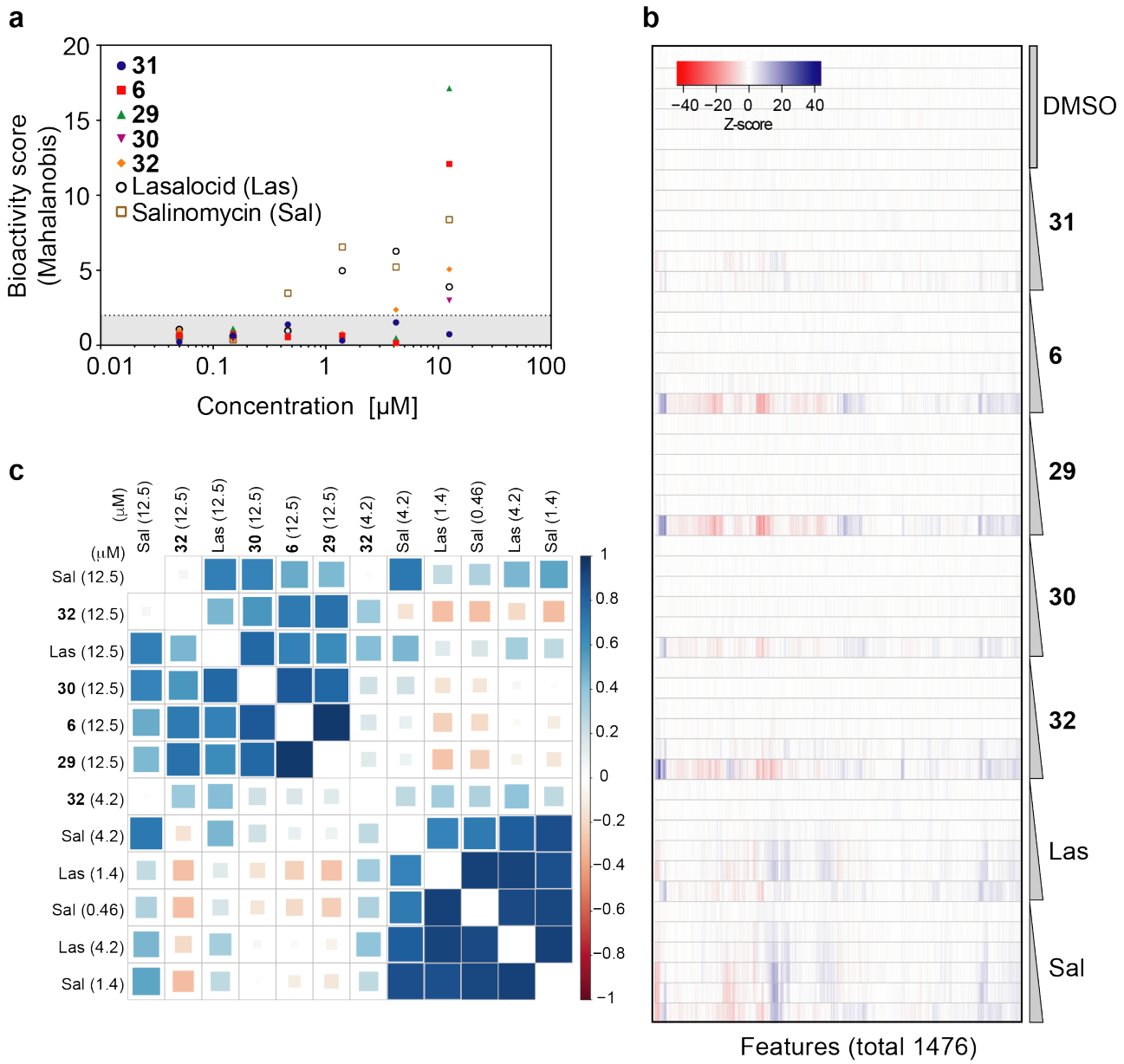

Figure 6. Morphological profiling. (a) Bioactivity scores as measured by the Mahalanobis distance to DMSO control. The grey area (Mahalanobis distance < 2) indicates inactivity. Sal and Las show activity at a lower concentration than the hybrid ionophores. (b) Heatmap of full morphological profiles. The color corresponds to the Z-score calculated from averaged profiles. **6**, **29**, **30** and **32** shows similar profiles at the highest concentration (12.5 μM). Note that the shown DMSO treatments are kept separate from the other DMSO controls used in the normalization step. (c) Pearson correlation matrix of active compounds ordered by hierarchical clustering. Two clusters with distinct bioactivities are formed, one containing lower

327 concentrations of Las and Sal and one containing high concentrations of both hybrid
328 ionophores and Las and Sal. The color and size of the squares indicates the Pearson correlation
329 coefficient.
330
331 All compounds were tested at six different concentrations (0.05-12.5 μM) and we used
332 salinomycin and lasalocid as controls. First, we calculated the Mahalanobis distance for all
333 compound treatments to DMSO controls as an overall measure for above-background activity
334 in the assay (Figure 6a and Figure S5-7). Using a rather strict threshold (see Supporting
335 Information for details and Fig. S6), hybrid polyethers **6**, **29** and **30** were scored inactive at all
336 but the highest concentration (12.5 μM), compound **32** had an active profile also at 4.2 μM, and
337 epimer **31** was inactive at all tested concentrations.
338 In contrast to the hybrid polyethers, salinomycin and lasalocid were both active at lower
339 concentrations (by 9-27 fold, Figure 6a). The full bioactivity profiles were plotted (Figure 6b)
340 and a Pearson correlation matrix was calculated for all compound treatments exceeding the
341 activity threshold (Figure 6c). We were quite surprised by the outcome of this analysis: The
342 activity profiles of salinomycin and lasalocid over several concentrations were clustered (*P*
343 0.83-0.94) whereas the hybrid ionophores – at the highest concentration – formed a distinct
344 cluster (Figure 6c). Interestingly, high concentrations of both lasalocid and salinomycin also
345 afforded profiles with significant correlations ($P > 0.63$) to this cluster as did a subset of a
346 reference panel of different growth inhibitory compounds (Figure S7) suggestive of a general
347 toxicity profile. In contrast, the bioactivity profiles associated with the first cluster (low
348 concentration Sal and Las) did not show significant correlations with profiles in our reference
349 panel.
350 Given the recent strong interest in the cellular activity of salinomycin[29,30,31] and the significant
351 difference in both the chemical structures and ionophore-properties associated with

352 salinomycin (a K-ionophore as previously mentioned) and lasalocid (a Ca-ionophore), the
353 apparent mechanistic similarity - which is suggested by our data - demands future attention.
354 Another important observation from these experiments is that the hybrid polyethers appear to
355 be more 'silent' in mammalian (U2OS) cells despite having similar anti-bacterial activity
356 compared to lasalocid and salinomycin.
357

358 **Discussion**

359 As we consider the potential future role of polyether ionophores in biomedicine the following
360 questions are important: 1) Can polyether ionophores be identified with a sufficiently large
361 therapeutic window to be considered as human antibiotics; 2) Can the activity of these
362 compounds be expanded to also target gram-negative strains; 3) Which aspects of mammalian
363 cell biology can be modulated by polyethers? To answer all of these questions, a large increase
364 in accessible compounds within the overall polyether-class is needed. For instance, systematic
365 tests in expanded bacterial panels may reveal activity patterns that can inform further
366 structural variations and in combination with investigations of cross-resistance to other
367 antibiotics new synthetic lead structures can be identified. The use of unbiased bioactivity
368 profiling in mammalian cells – as we demonstrate here – may both pinpoint polyethers with
369 unusual activity patterns that can be subjected to focused mechanistic investigations as well as
370 variants that appear 'silent' in mammalian cells while maintaining antibacterial activity. Hybrid
371 polyether **29** is a good example of the latter. The compound has a ratio of 0.5 between the
372 average (molar) MIC across the *S. aureus* strains and the first bioactive concentration in U2OS
373 cells whereas the equivalent numbers for salinomycin and lasalocid are 5.8 and 2.4,
374 respectively. However, we currently do not understand the mechanistic and structural factors
375 that underlie these differences. On a similar note, despite having closely related structures,
376 compounds **6** and **29** are less active (up to 64 fold) compared to the remarkably low MIC-values

377 reported for ecteinamycin (**2**)[36]. The specific reason(s) for this difference is also of strong
378 interest. We e.g. note that in the solid state, the sodium-bound forms of **2** and **6/29** differ subtly
379 due to the structural variations close to the C17-C18 bond (Figure S8). How these changes affect
380 the relative selectivity and efficiency of ion-transport should be addressed in future studies.
381 In conclusion, it is evident that complex polyethers can affect both eukaryotic and prokaryotic
382 cells in ways that transcend the canonical model of pleiotropic ion-transporters and therefore
383 that a strategic merger of synthesis and biology broadly across this class of compounds is
384 timely. The overall synthesis principle of reusing parts of the abundant polyethers that we
385 outline in this paper - fueled by novel methods (such as MicroED[55]) to expedite structural
386 assignment of complex molecules and methods to study mechanisms-of-action - may therefore
387 contribute to the effective resurrection of this whole class of compounds.
388

389 **Acknowledgements**

390 TBP acknowledges financial support from the Carlsberg foundation (grant CF17-0800) and
391 Independent Research Fund Denmark (Sapere Aude 2 grant 6110-00600A). We are grateful to
392 Eric Jung and Anja Johnbeck for technical assistance with organic synthesis, Anders Bodholt
393 Nielsen for technical assistance with NMR spectroscopy, and Iben Charlotte Stensgaard Jensen
394 for technical assistance with microbiology.
395

396 **Author contributions**

397 TBP conceived and supervised the study. TBP, SL, and HL designed experiments. SL, HL, and
398 CNP performed organic synthesis. EBS conducted cell biological experiments and analyzed
399 data. TT supervised microbiology experiments and analyzed data. PN carried out x-ray
400 crystallographic analyses. TBP, SL, HL wrote the manuscript with input from all authors.
401

402 **Competing financial interests**

403 The authors declare no competing financial interests

404

405 **Methods**

406 **Organic Synthesis**

407 All reactions were conducted in flame-dried glassware under an atmosphere of argon unless
408 otherwise stated. CH_2Cl_2, MeCN, THF and PhMe were dried over aluminium oxide via an
409 MBraun SPS-800 solvent purification system. DCE, DMF, MeOH and pyridine were purchased
410 as anhydrous. The dryness of solvents was controlled via Karl Fischer tritration. Reagents were
411 used as received from commercial suppliers unless otherwise stated (Sigma Aldrich, Merck, AK
412 Scientific, and Fluorochem). Et_3N and DIPEA were dried by stirring for at least 30 minutes over
413 CaH_2 followed by distillation onto preactivated molecular sieves (4 Å). Concentration *in vacuo*
414 was performed using a rotary evaporator with the water bath temperature at 30 °C, or 40 °C,
415 followed by further concentration using a high vacuum pump. TLC analysis was carried out on
416 silica coated aluminum foil plates (Merck Kieselgel 60 F254). The TLC plates were visualized
417 by UV irradiation and/or by staining with either CAM stain ($(NH_4)_6Mo_7O_{24}\cdot 4H_2O$ (10 g), Cerric
418 ammonium sulfate (4 g), 10% H_2SO_4 (aq., 400 mL)), ninhydrin stain (ninhydrin (12 g) and AcOH
419 (12 mL) in *n*-butanol (400 mL)) or $KMnO_4$ stain ($KMnO_4$ (5.0 g), 5 % NaOH (aq., 8.3 mL) and
420 K_2CO_3 (33.3 g) in H_2O (500 mL)). Molecular sieves were activated by drying in the oven at 120
421 °C for at least 24 hours, before they were heated in a microwave at maximum power for 2
422 minute, followed by evaporation of the formed vapour on the high vacuum line. This was
423 repeated 3-4 times, and finished by gently flame-drying the flask containing the molecular
424 sieves. Flash column chromatography (FCC) was carried out using silica gel (230-400 mesh
425 particle size, 60 Å pore size) as stationary phase. Infrared spectra (IR) were acquired on a
426 PerkinElmer Spectrum TwoTM UATR. Mass spectra (HRMS) were recorded on a Bruker
427 Daltonics MicrOTOF time-of-flight spectrometer with positive electrospray ionization, or

428 negative ionization when stated. Nuclear magnetic resonance (NMR) spectra were recorded on
429 a Varian Mercury 400 MHz spectrometer or a Bruker BioSpin GmbH 400 MHz spectrometer,
430 running at 400 and 101 MHz for ^{1}H and ^{13}C, respectively. Chemical shifts (δ) are reported in
431 ppm relative to the residual solvent signals ($CDCl_3$: 7.26 ppm ^{1}H NMR, 77.16 ppm ^{13}C NMR,
432 CD_3OD: 3.31 ppm ^{1}H NMR, 49.00 ppm ^{13}C NMR, ^{6}d-DMSO: 2.50 ppm ^{1}H NMR, 39.52 ppm ^{13}C
433 NMR. Multiplicities are indicated using the following abbreviations: s = singlet, d = doublet, t =
434 triplet, q = quartet, h = heptet, m = multiplet, br = broad. LC-MS and HPLC analysis and
435 purification were performed using a Gilson HPLC system.
436
437 For all remaining methods, see the supplementary information.
438
439 **References**

[1] A. Agtarap, J. Chamberlin, J. W. Pinkerton and L. Steinrauf, *J. Am. Chem. Soc.*, **89**, 5737 (1967).

[2] Westley, J. ed., (1982). *Polyether Antibiotics - Naturally Occurring Acid Ionophores*. 1st ed. New York: Marcel Dekker.

[3] Dutton, C. J., Banks, B. J. & Cooper, C. B. Polyether ionophores. *Nat. Prod. Rep.* **12,** 165–181 (1995).

[4] Nakata, T. *et al.* A Total Synthesis of Lasalocid A. *J. Am. Chem. Soc.* **100,** 2933–2935 (1978).

[5] Fukuyama, T. *et al.* Total Synthesis of Monensin. 3. Stereocontrolled Total Synthesis of Monensin. *J. Am. Chem. Soc.* **101,** 262–263 (1979).

[6] Collum, D. B., McDonald, J. H. & Still, W. C. Synthesis of the Polyether Antibiotic Monensin. 3. Coupling of Precursors and Transformation to Monensin1. *J. Am. Chem. Soc.* **102,** 2120–2121 (1980).

[7] Ireland, R. E., Thaisrivongs, S. & Wilcox, C. S. Total Synthesis of Lasalocid A (X537A). *J. Am. Chem. Soc.* **102,** 1155–1157 (1980).

[8] Evans, D. A., Bender, S. L. & Morris, J. Total Synthesis of the Polyether Antibiotic X-206. *J. Am. Chem. Soc.* **110,** 2506–2526 (1988).

[9] Corey, E. J. & Cheng, X.-M. *The logic of chemical synthesis*. (Wiley, 1995).

[10] Faul, M. M. & Huff, B. E. Strategy and Methodology Development for the Total Synthesis of Polyether Ionophore Antibiotics. *Chem. Rev.* **100,** 2407–2473 (2000).
[11] Song, Z., Lohse, A. G. & Hsung, R. P. Challenges in the synthesis of a unique mono-carboxylic acid antibiotic, (+)-zincophorin. *Nat. Prod. Rep.* **26,** 560–571 (2009).
[12] Liu, H., Lin, S., Jacobsen, K. M. & Poulsen, T. B. Chemical syntheses and chemical genetics of carboxyl polyether ionophores: Recent highlights, *Angew. Chem. Int. Ed.* (2019), doi: 10.1002/anie.201812982
[13] Schwan, J. & Christmann, M. Enabling strategies for step efficient syntheses. *Chem. Soc. Rev.* **47,** 7985–7995 (2018).
[14] Gaich, T. & Baran, P. S. Aiming for the ideal synthesis. *J. Org. Chem.* **75,** 4657–4673 (2010).
[15] Kasun, Z. A., Gao, X., Lipinski, R. M. & Krische, M. J. Direct Generation of Triketide Stereopolyads via Merged Redox-Construction Events: Total Synthesis of (+)-Zincophorin Methyl Ester. *J. Am. Chem. Soc.* **137,** 8900–8903 (2015).
[16] Wang, G. & Krische, M. J. Total Synthesis of (+)-SCH 351448: Efficiency via Chemoselectivity and Redox-Economy Powered by Metal Catalysis. *J. Am. Chem. Soc.* **138,** 8088–8091 (2016).
[17] Chen, L.-A., Ashley, M. A. & Leighton, J. L. Evolution of an Efficient and Scalable Nine-Step (Longest Linear Sequence) Synthesis of Zincophorin Methyl Ester. *J. Am. Chem. Soc.* **139,** 4568–4573 (2017).
[18] Huffman, B. J. & Shenvi, R. A. Natural Products in the 'Marketplace': Interfacing Synthesis and Biology. *J. Am. Chem. Soc.* **141**, 3332–3346 (2019).
[19] Schreiber, S. L. Target-oriented and diversity-oriented organic synthesis in drug discovery. *Science* **287,** 1964–1969 (2000).
[20] Wetzel, S., Bon, R. S., Kumar, K. & Waldmann, H. Biology-oriented synthesis. *Angew. Chem. Int. Ed.* **50,** 10800–10826 (2011).
[21] Könst, Z. A. *et al.* Synthesis facilitates an understanding of the structural basis for translation inhibition by the lissoclimides. *Nat. Chem.* **9,** 1140–1149 (2017).
[22] Wilson, R. M. & Danishefsky, S. J. Small molecule natural products in the discovery of therapeutic agents: the synthesis connection. *J. Org. Chem.* 71, 8329–8351 (2006).
[23] Huigens, R. W. *et al.* A ring-distortion strategy to construct stereochemically complex and structurally diverse compounds from natural products. *Nat. Chem.* **5,** 195–202 (2013).
[24] Abbasov, M. E. *et al.* Simplified immunosuppressive and neuroprotective agents based on gracilin A. *Nat. Chem.* **11,** 342–350 (2019).
[25] Seiple, I. B. *et al.* A platform for the discovery of new macrolide antibiotics. *Nature* **533,** 338–345 (2016).

[26] Richter, M. F. *et al.* Predictive compound accumulation rules yield a broad-spectrum antibiotic. *Nature* **545,** 299–304 (2017).

[27] Focused analogs of polyether ionophores have been made. See especially ref. 2. A recent example for salinomycin: Antoszczak, M. et al. Biological activity of doubly modified salinomycin analogs - Evaluation in vitro and ex vivo, *Eur. J. Med. Chem.* 156, 510–523 (2018).

[28] Versini, A. *et al.* Chemical biology of salinomycin. *Tetrahedron* **74,** 5585–5614 (2018).

[29] Gupta, P. B. *et al.* Identification of selective inhibitors of cancer stem cells by high-throughput screening. *Cell* **138,** 645–659 (2009).

[30] Mai, T. T. *et al.* Salinomycin kills cancer stem cells by sequestering iron in lysosomes. *Nat. Chem.* **9,** 1025–1033 (2017).

[31] Wang, F. *et al.* Nucleolin Is a Functional Binding Protein for Salinomycin in Neuroblastoma Stem Cells. *J. Am. Chem. Soc.* **141**, 3613–3622 (2019).

[32] Chapman, H. D., Jeffers, T. K. & Williams, R. B. Forty years of monensin for the control of coccidiosis in poultry, *Poultry Sci.* **89**, 1788–1801 (2010).

[33] Goodrich, R. D. et al. Influence of monensin on the performance of cattle. *J. Anim. Sci.* **58**, 1484–1498 (1984).

[34] Kevin II, D. A., Meujo, D. A. & Hamann, M. T. Polyether ionophores: broad-spectrum and promising biologically active molecules for the control of drug-resistant bacteria and parasites. *Expert Opin. Drug Discov.* **4**, 109–146 (2009)

[35] Igarashi, Y. *et al.* Nonthmicin, a Polyether Polyketide Bearing a Halogen-Modified Tetronate with Neuroprotective and Antiinvasive Activity from Actinomadura sp. *Org. Lett.* **19,** 1406–1409 (2017).

[36] Wyche, T. P. *et al.* Chemical Genomics, Structure Elucidation, and in Vivo Studies of the Marine-Derived Anticlostridial Ecteinamycin. *ACS Chem. Biol.* **12,** 2287–2295 (2017).

[37] Westley, J. W., Evans, R. H., Williams, T. & Stempel, A. Structure of antibiotic X-537A. *J. Chem. Soc. D*, 71–72 (1970).

[38] Westley, J. W., Evans, R. H., Williams, T. & Stempel, A. Pyrolytic Cleavage of Antibiotic X-537A and Related Reactions. *J. Org. Chem.* **38,** 3431–3433 (1973).

[39] Gruenfeld, N. *et al*. Angiotensin Converting Enzyme Inhibitors: Derivatives l-Glutarylindoline-2-carboxylic Acid. *J. Med. Chem.* **26**, 1277–1282 (1983).

[40] Lautens, M., Colucci, J. T., Hiebert, S. & Smith, N. D. Total Synthesis of Ionomycin Using Ring-Opening Strategies. *Org. Lett.* **4**, 1879–1882 (2002)

[41] Mico, A. D., Margarita, R., Parlanti, L., Vescovi, A. & Piancatelli, G. A Versatile and Highly Selective Hypervalent Iodine (III)/2,2,6,6-Tetramethyl-1-piperidinyloxyl-Mediated Oxidation of Alcohols to Carbonyl Compounds. *J. Org. Chem.* **62,** 6974–6977 (1997).

[42] Zhang, Z. & Tong, R. Synthetic Approaches to 2, 6-*trans*-Tetrahydropyrans. *Synthesis* **49**, 4899–4916 (2017).

[43] Brazeau, J.-F. *et al*. Stereocentrolled Synthesis of C1-C17 Fragment of Narasin via a Free Radical-Based Approach. *Org. Lett.* **12**, 36–39 (2010).

[44] Hiyama, T., Kimura, K. & Nozaki, H. Chromium (II) Mediated Threo Selective Synthesis of Homoallyl Alcohols *Tetrahedron Lett.* **22**, 1037–1040 (1981).

[45] Hansen, T. M. *et al*. Highly Chmoselective Oxidation of 1, 5-diols to δ-lactones with TEMPO/BAIB. *Tetrahedron Lett.* **44**, 57–59 (2003)

[40] Zografos, A. L. & Georgiadis, D. Synthetic strategies towards naturally occurring tetronic acids. *Synthesis* 3157–3188 (2006).

[41] Schobert, R. & Jagusch, C. Solution-phase and solid-phase syntheses of enzyme inhibitor RK-682 and antibiotic agglomerins. *J. Org. Chem.* **79**, 6129–6132 (2005).

[42] Hori, K., Hikage, N., Inagaki, A., Mori, S., Nomura, K. & Yoshii, E. Total synthesis of tetronomycin. *J. Org. Chem.* **57**, 2888–2902 (1992).

[43] Tatsuta, K., Suzuki, Y., Furuyama, A. & Ikegami, H. The first total synthesis of a tetracyclic antibiotic, (-)-tetrodecamycin. *Tetrahedron Lett.* **47**, 3595–3598 (2006).

[44] Markó, I. E., Richardson, P. R., Bailey, M., Maguire, A. R. & Coughlan, N. Selective manganese-mediated transformations using the combination: $KMnO_4/Me_3SiCl$. *Tetrahedron Lett.* **38**, 2339–2342 (1997).

[45] Sabbah, M., Bernollin, M., Doutheau, A., Soulère, L. & Queneau, Y. *Med. Chem. Commun.* **4**, 363–366 (2013).

[46] Roush, W. R. Concerning the Diastereofacial Selectivity of the Aldol Reactions of α-Methyl Chiral Aldehydes and Lithium and Boron Propionate Enolates. *J. Org. Chem.* **56,** 4151–4157 (1991).

[47] Masamune, S., Choy, W., Petersen, J. S. & Sita, L. R. Double Asymmetric Synthesis and a New Strategy for Stereochemical Control in Organic Synthesis. *Angew. Chem. Int. Ed.* **24,** 1–30 (1985).

[48] Heathcock, C. H. & Flippin, L. A. Acyclic Stereoselection. 16. High Diastereofacial Selectivity in Lewis Acid Mediated Additions of Enolsilanes to Chiral Aldehydes. *J. Am. Chem. Soc.* **105,** 1667–1668 (1983).

[49] Evans, D. A., Yang, M. G., Dart, M. J., Duffy, J. L. & Kim, A. S. Double Stereodifferentiating Lewis Acid-Promoted (Mukaiyama) Aldol Bond Constructions. *J. Am. Chem. Soc.* **117,** 9598–9599 (1995).

[50] Nicolaou, K. C., Estrada, A. A., Zak, M., Lee, S. H., Safina, B. S. A mild and selective method for the hydrolysis of esters with trimethyltin hydroxide, *Angew. Chem. Int. Ed.* **44**, 1378–1382 (2005)

[51] Hoffmann, R. W., Conformation design of open-chain compounds, *Angew. Chem. Int. Ed.* **39**, 2054–2070 (2000)

[52] Evans, D., Chapman, K. & Carreira, E. Directed reduction of β-hydroxy ketones employing tetramethylammonium triacetoxylborohydride. *J. Am. Chem. Soc.* **110**, 3560–3578 (1988).

[53] Bray, M.-A. *et al.* Cell Painting, a high-content image-based assay for morphological profiling using multiplexed fluorescent dyes. *Nat. Protoc.* **11,** 1757–1774 (2016).

[54] Svenningsen, E. B. & Poulsen, T. B. Establishing cell painting in a smaller chemical biology lab – A report from the frontier. *Bioorg. Med. Chem.* **27**, 2609–2615 (2019).

[55] Nannenga, B. L. & Gonen, T. The cryo-EM method microcrystal electron diffraction (MicroED). *Nat. Meth.* **16,** 369–379 (2019).